CHAPTER 19

Using Green Fluorescent Protein Fusion Proteins to Quantitate Microtubule and Spindle Dynamics in Budding Yeast

Kerry S. Bloom, Dale L. Beach, Paul Maddox, Sidney L. Shaw,* Elaine Yeh, and Edward D. Salmon

Department of Biology
University of North Carolina at Chapel Hill
Chapel Hill, North Carolina 27599-3280

* HHMI Long Laboratory
Department of Biology
Stanford University
Stanford, California 94305

I. Introduction

The small cell size and susceptibility to photodamage complicate imaging live budding yeast. The haploid yeast cell measures only 5–8 μm in diameter, requiring

METHOD
Copyright
1091-679X

that high magnification and high numerical aperture lenses be used for resolution of intracellular structures. Furthermore, yeast have little intrinsic contrast, requiring the use of differential interference contrast (DIC) optic for brightfield imaging. Fluorescence studies of Green fluorescent protein (GFP) fusion proteins are difficult because high-intensity excitation at 470 nm or shorter wavelengths for more than 2 or 3 min dramatically impairs cell growth and results in GFP photobleaching.

The previous conditions present a serious problem for the microscopist. Fluorescence excitation must be of low intensity to prevent phototoxicity and photobleaching during the course of a time-lapse experiment. Also, the level of GFP fusion protein expression must be kept low so that excess protein does not adversely affect the cell. Under these conditions, the total light from GFP fluorescence emmission is extremely small. Compounding the problem is the requirement for high magnification. As total magnification increases, the amount of light collected at the microscope decreases as a product of the square of the magnification. Gathering sufficient fluorescence signal for imaging without damaging the cells requires that the efficiency of the optical system be maximized and necessitates balancing temporal and spatial resolution with the need for light sensitivity.

One project that illustrates both the difficulties and the potential benefits of imaging GFP fusion proteins in live yeast cells is the problem of how microtubules contribute to the positioning of the nucleus. The astral microtubules in budding yeast are very labile and have been difficult to preserve by fixation methods for either immunofluorescence or electron microscopy. We have developed a C-terminal dynein–GFP probe (Shaw *et al.*, 1997b) containing an N-terminal 300-amino acid deletion, which partially complements dynein null mutants. This probe labels the astral microtubules, which have a role in moving the nucleus to the nascent bud. Characterizing the astral microtubule assembly dynamics using the dynein–GFP probe required that we optimize our handling of GFP expressing cells and dictated several microscopy enhancements to allow imaging over the 90+ min cell cycle. In addition, it was imperative to examine cells with similar amounts of the dynein–GFP fusion protein, necessitating a quantitative measurement of fluorescence in single cells.

The multimode instrumentation we developed for time-lapse GFP, DIC, and DAPI imaging has been presented in detail elsewhere (Salmon *et al.*, 1998; Shaw *et al.*, 1997a). This article focuses on aspects of cloning, with regard to promoter choice for GFP fusion proteins, methods to quantitate the fluorescence signal in single cells, and quantitative solutions to the imaging problem. Examples of cells expressing excess levels of dynein–GFP are provided to illustrate (i) how overexpression is documented and (ii) phenotypes resulting from severe protein overexpression.

II. Construction of Protein–GFP Fusion and Promoter Selection

Several modules for construction of GFP fusion proteins have been reported hat allow very rapid one-step manipulation without requiring plasmid clones of

the gene of interest. These modules utilize the regulatable HIS3 (Straight *et al.*, 1996, 1997), MET25 (Mumberg *et al.*, 1994; Niedenthal *et al.*, 1996), or GAL1–10 (Longtine *et al.*, 1998) promoters. Endogenous promoters that drive sufficient quantities for visualization include Nuf2p (Kahana *et al.*, 1995), Myo1p (Bi *et al.*, 1998; Lippincott and Li, 1998), Sec3p (Finger *et al.*, 1998), Tub3p (S. Shaw and K. Bloom, unpublished results), and Tublp (A. Straight, personal communication). However, many GFP–protein fusions (i.e., dynein) have not been visualized with endogenous promoters and therefore require methods to enhance mRNA transcription.

A. Choice of Vector Cassette

Levels of GFP fusion proteins are dependent in part on the plasmid vector containing the expression cassette. Integrative vectors offer the benefit of a single copy in every cell. Advantages include uniform copy number and the presence of the clone throughout the population. Plasmids maintained with centromere DNA are present in 2–5 copies per cell (Futcher and Carbon, 1986; Resnick *et al.*, 1990). Centromere plasmids are present in a very large fraction of the population (>80% depending on the growth conditions). Using the 2μ vector can increase copy number to 40–60 copies per cell, with concomitant increases in expression levels (Mumberg *et al.*, 1994). Variation in the copy number of these plasmids from cell to cell may contribute to the heterogeneity in expression levels seen in single cells of a population.

B. Choice of Promoter

The ability to regulate the quantity of GFP–fusion protein in individual cells is paramount to obtaining an accurate assessment of protein function. Saturation of binding sites by excess levels of the fusion protein may contribute to background fluorescence or lead to aberrant positioning of the fusion protein *in vivo*. The level of mRNA transcription, and thus protein level, is greatly influenced by the strength of the promoter. Low-level constitutive promoters, such as the actin promoter, can produce sufficient amounts of protein without the need for induction (Amberg *et al.*, 1997). Transcription from many regulatable promoters ranges from low to titratable and extremely high levels. The HIS3 promoter exhibits very low levels of transcription in the presence of histidine, basal levels of expression during histidine starvation, and enhanced expression with addition of 3-aminotriazole (3-AT), a competitive inhibitor of histidine (Straight *et al.*, 1996). Bimodal expression levels from the HIS3 promoter derive from amino acid starvation (about 10-fold increase) and global amino acid derepression (triggered by 3-aminotriazole as well as amino acid imbalances) increasing transcription an additional 2.5- to 4-fold (Hinnebusch, 1992; Jones and Fink, 1982).

The MET promoter can be titrated with methionine to produce a linear gradient of expression. Below a threshold of 500 μM methionine, the MET25 promoter increases protein amounts nearly linearly to fourfold baseline levels as methio-

nine concentration decreases in the media (Mumberg *et al.*, 1994). Thus, levels of GFP fusion protein can be adjusted to optimize levels of signal over background fluorescence. Additionally, varying the methionine concentration of the media during imaging maintains induction over the course of the experiment. Appropriate levels of induction during imaging must be determined empirically. This may be critical for proteins with short half-lives or to replenish photobleached GFP molecules to endogenous levels. The MET promoter is comparable to other variably active promoters, such as CUP1 (Etcheverry, 1990; Resnick *et al.*, 1990), in its ability to regulate levels of gene product. The MET25 promoter, and the use of amino acid starvation to regulate gene activity, compares favorably to heavy metal salts, which may further stress cells during imaging.

The divergent GAL1–10 promoter is one of the most highly active promoters, generating a level of expression on the order of 1000 times more than the uninduced state. In addition, catabolite repression in cells grown on glucose renders the promoter virtually incapacitated. In this way, high levels of expression on galactose and tight repression on glucose can be attained. A consequence of the catabolite repression is that stores of glucose must be depleted prior to activation by galactose. A temporal lag in induction occurs following addition of galactose to a glucose-grown culture. This can be avioded by growing cells on carbon sources that do not induce catabolite repression, such as raffinose or sucrose.

It has been reported that levels of expression from GAL1 promoter can be regulated by altering the ratio of galactose : glucose in the medium (Moreland *et al.*, 1987). This provides another option in the repertoire of induction strategies. It is likely that a small amount of glucose in the presence of galactose delays induction from the GAL1 promoter. It is of interest to determine the levels of induction in single cells grown in varying galactose : glucose cultures. Once an individual cell induced, the levels of induction might be comparable to and independent of the galactose : glucose ratio in the medium. In any case, induction for extended periods of time is not recommended because overexpression and excess accumulation of fusion protein is likely to be detriment

Inducing Production of the GFP Fusion Protein

The induction regime for visualizing GFP fusion proteins is critical for success in subsequent analysis. It is essential for cells to be in midlogarithmic growth phase because this will increase the likelihood of survival during the imaging process. In our experience, very short induction times have been sufficient (and are optimal) in obtaining visible levels of a GFP fusion protein. Addition of galactose to raffinose-grown cultures results in very rapid (15 min) induction from the GAL1 promoter. Thirty-minute induction from the HIS3 promoter (following addition of 3-AT) leads to detectable levels of signal with low background (Straight *et al.*, 1996, 1997). Expression from the MET25 promoter requires 1.5–3 hr of induction to obtain renderable levels of fluorescence. Typically,

cells grown to early or midlogarithmic growth phase can be switched into inducing conditions without a significant lag in growth and then harvested after an appropriate time for microscopy.

III. Quantifying Fluorescence in Cell Populations

Quantification of fluorescence intensity by flow cytometry of cells expressing GFP from the GAL1, GAL4, and URA3 promoters produced bell-shaped curves representing the distribution of fluorescence in a population of cells (Niedenthal *et al.*, 1996). Cells not expressing GFP also displayed a bell-shaped curve reflecting the distribution of autofluorescence in uninduced populations. Induction levels were evident by the peaks of separation in the autofluorescence versus induced fluorescence. GFP production from the strong GAL1 promoter increased the peak of fluorescent intensity 10-fold over autofluorescence, therefore reducing the overlap between the two curves. Expression from the GAL4 or URA3 promoters provided minimal separation between induced and uninduced levels of fluorescence. Such differences provide clear indications of promoter strength and illustrate the gains in expression when "strong" promoters are used to drive expression of the fusion protein. Production of GFP fusion protein above autofluorescence is fundamental to one's ability to resolve localized protein in the cell; however, the trade-offs of overexpression are potentially detrimental side effects for certain proteins.

The fluorescence measurements provide an accurate assessment of protein concentration. When a GFP fusion to a TATA-binding protein was imaged by quantitative laser scanning confocal microscopy (LSCM), the levels measured by LSCM correlated with the levels determined by immunoblot of whole cell extract protein (Patterson and Piston, 1998). Thus, the live cell analysis provides a new dimension in this genetic system. However, it is imperative that precise fluorescence measurements be made to ensure that individual cells being examined express similar amounts of the fusion protein. Imaging GFP fusion proteins not only offers a method of measurement equivalent to a more conventional technique but also provides real-time quantitation.

A. Quantitative Image Analysis of Fluorescence Intensity in Single Cells

Changes in expression level of tubulin and/or microtubule motors have significant consequences on microtubule dynamics. Altered stoichiometry of tubulin has dire effects on cell growth (Solomon, 1991). Likewise, alterations in motor proteins may adversely affect microtubule dynamics, such as changes in growth or shortening velocities, or frequency of rescue (Shaw *et al.*, 1997b). As shown in Fig. 1, the heterogeneity in single cells expressing a bacteriophage MS2–GFP fusion protein is quite significant. For accurate kinetic measurements, it is critical that one examines cells expressing similar concentrations of the fusion protein.

A

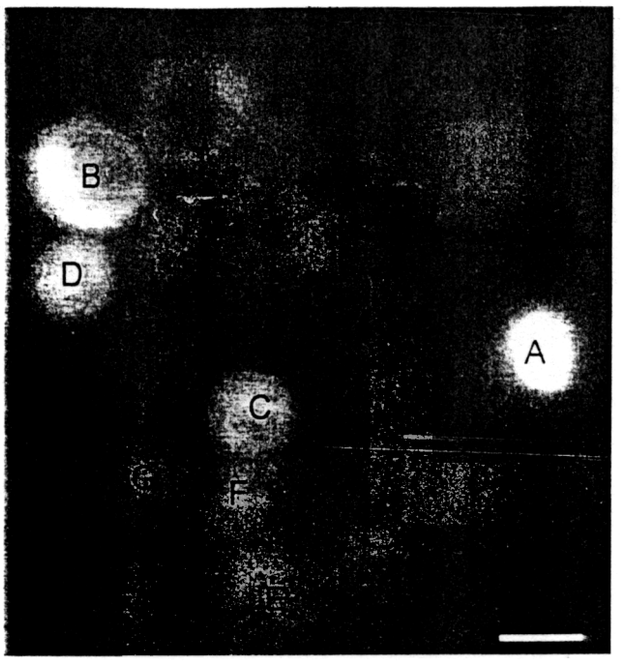

B

CELL	RF	CELL	RF
. .	>4095	F	2544
		G	
		H	
D		I	
		BG	

Fig. 1 Individual cells in large population may exhibit heterogeneity in protein levels. (A) Expression from the MET25 promoter (2 hr of induction) of a cytoplasmic protein (the bacteriophage MS2 coat protein) fused to GFP leads to a virtually continuous range of fluorescent intensities in individual cells. The cells with no fluorescence most likely represent plasmid loss (the fraction of cells lacking fluorescence correlates to the fraction of cells without plasmid). (B) Measurements of the relative fluorescence (RF) for each labeled cell. The arbitrary units correspond to pixel values also known as gray level. Cell A exceeds the maximum gray level in this exposure. A background reading (BG) was taken from the lower right corner of the image. Variation of fluorescence in the population is likely to be related to plasmid copy number and variations in transcriptional activity. Scale μm.

To measure the protein levels in single cells, all images should be unenhanced since enhancement of contrast or brightness changes the intensity value. The maximum, minimum, and average intensity of the fluorescence should be recorded as well as the imaging conditions (exposure time, excitation intensity,

camera settings, and lens elements used), making sure that maximum intensity is less than the saturation level of the camera. These measurements result in a range of intensity, which correlates directly with expression levels.

Once the range has been established, the level of protein expression in which the kinetic phenotype is complemented can be deduced. For our purposes, dynein–GFP is expressed in cells lacking the endogenous dynein gene (a dynein null background). Exogenous expression of dynein–GFP results in three major phenotypes. The first is underexpression, i.e., the expression of dynein–GFP is insufficient to complement the mutant phenotype. The second is overexpression, resulting in growth defects and malpositioning of the mitotic spindle (Shaw *et al.*, 1997b). Finally, there is a range of expression between these two phenotypes that provides sufficient dynein to restore wild-type spindle movement and kinetic progression through mitosis. Since expression is heterogeneous within a given population of cells, we posit that complementation in individual cells expressing specified level of protein expression be the standard for such experiments.

By comparing the relative fluorescence within various cells and observing the doubling time of these cells, a standard can be determined for the amount of GFP fusion protein that does not perturb the kinetics of cell cycle progression. The relative amount of GFP fusion protein can be determined by measuring the mean and maximum pixel value (gray level or fluorescence intensity in arbitrary units) within a given cell as seen in unenhanced images. Various points of fluorescence, such as spindle poles and microtubules, should be measured and compared throughout the population to ensure accuracy. Cells observed by time-lapse microscopy can then be analyzed for growth rate versus expression level. Using the expression standard allows a high level of assurance that the reported experimental observations are derived from cells with wild-type growth rates (Shaw *et al.*, 1997b). Cells that are expressing a level of GFP fusion protein determined to be deleterious to the cell (such as slowed cell cycle time) can be excluded from further study.

IV The Imaging System

Our digital imaging microscope utilizes conventional wide-field optics and a cooled, slow-scan charge couple device (CCD) camera for image detection (Fig. 2). Because we require both DIC and fluorescence images, a filter wheel containing an analyzer and a glass blank (to equalize the light path for DIC and fluorescence modes) has been placed in front of the CCD camera to assist in switching between DIC and fluorescence modes. Filters and shutters have been added to the microscope to control light intensity for both DIC and fluorescence illumination pathways. A multiple bandpass dichromatic mirror in combination with an excitation filter wheel is used to rapidly switch between GFP and DAPI imaging. Focus is controlled by hand or by using an electronic focus motor. Most aspects (shutters, filter wheels, and focus) of the microscope have been automated and are con-

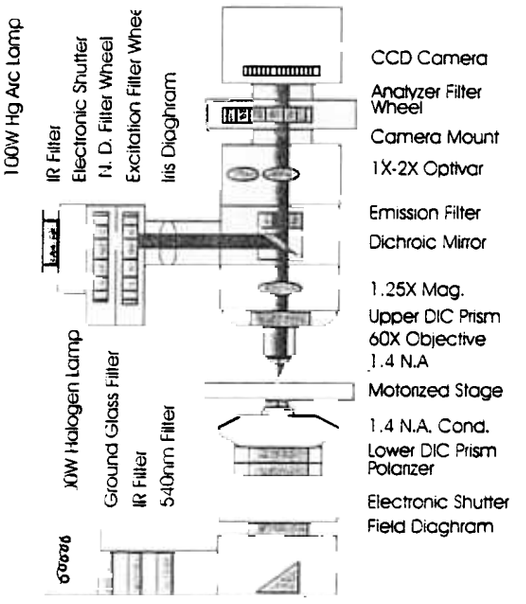

Fig. 2 Multimode optical microscope. Modification of our original imaging system (for component list, see Salmon *et al.*, 1994) by the addition of a filter wheel containing the DIC analyzer allowed automated switching between DIC and fluorescent modes (Salmon *et al.*, 1998). NA, numerical aperture; ND, neutral density.

trolled by Pentium-based computer system running MetaMorph software developed by Universal Imaging Corporation. The system is explained in detail elsewhere (Shaw *et al.*, 1997a).

V Quantitative Solution to the Imaging Problem

A. Signal and Noise

Production of an image requires that more photoelectrons be collected from the specimen (signal) than from other sources (noise). Signal acquisition is a product of the number of fluorochromes (GFP molecules), the fluorescence excitation intensity, the quantum efficiency of the detector, and the duration of the exposure. GFP fusion concentration and fluorescence excitation must be very low to approach normal cell growth. The quantum efficiency of the CCD detector is fixed, leaving only the duration of the exposure as a variable for acquiring signal.

Noise in the imaging system derives from three major sources: autofluorescence and scattered light in the microscope system, the random nature of photon

generation, and the camera. Noise from scattered light in the microscope and from out of focus fluorescence in the media is substantially reduced by closing the epifluorescence field diaphragm to exclude all but the cell of interest. Noise is also reduced by placing the microscope in a dark room with minimal exposure to light from computer monitors.

Photons from the GFP molecule are emitted in a stochastic manner, not a steady stream, giving rise to "shot noise" or "photon noise" (Salmon *et al.*, 1998). This phenomena, measured as the square root of the total number of photons emitted, results in a variation on gray level values for the same pixel position from image to image. For example, if 100 photoelectrons are collected on average in one pixel well, the noise associated with that pixel is ± 10 electrons. In our system, 5 electrons correspond to 1 gray level, a difference of ± 2 gray levels of 20 between subsequent images for the same number of GFP molecules. When 1000 photoelectrons are collected, there is a ± 31 electron variability. Hence, as a percentage of signal, photon noise constitutes a maximum of 6% at 1000 photons (12 of 200 gray levels) but represents 20% at 100 photons (4 of 20 gray levels).

Camera noise comes from the amplifiers, which force the electrons out of the CCD wells into the computer (readout noise), and electrons arising from the silicon chip due to heat (dark current or thermal noise). Since the average camera noise for any given exposure time is generally a constant, we can later subtract this from our image using background subtraction. The standard deviation of the average represents the number of random electrons contributed to each well. The gray levels representing these electrons cannot be removed by background subtraction and appear as a variation in gray level for each image. Readout noise from the CCD chip is reduced by using "slow-scan" readout amplifiers. Dark current noise can be nearly eliminated by physically cooling the CCD chip. In our camera cooled to $-40°C$, the camera noise derives mainly from readout (about 10 electrons/pixel).

B. Resolution and Magnification

A 1.4 numerical aperture (NA) lens has a theoretical lateral resolving power for 540 nm light of about 235 nm. Hence, an 8-μm yeast cell divides into about 34 resolvable points along a line. Our CCD chip is composed of wells, or pixels, that are physically 12 μm square. By using 150× magnification, we project an 8-mm long yeast cell at a size of 1200 μm onto the CCD chip that, given the 12-μm pixel size, samples 100 points across the cell. Having 3 pixels per resolved unit satisfies the sampling criteria (Nyquist limit) for ensuring that we are accurately sampling all the resolvable information (Inoué and Spring, 1997).

In order to gain sensitivity for our fluorescence images we binned (grouped) the pixels on the chip 2×2 during readout, giving a pixel size of 24 μm square. The GFP or DAPI image is now sampled by only 50 pixels, whereas, the bright field image is still sampled by 100 pixels. The resolution of the fluorescence images is now limited by the camera and not by the microscope. Given that we

need two or three sample points for every unit of the resolution, our effective resolution is now between 320 and 480 nm for the fluorescence images. By binning the wells in the CCD chip, we sacrificed half of the spatial resolution in fluorescence for a fourfold increase in light sensitivity.

C. Imaging GFP in Live Cells with a CCD Camera

The main advantage of the CCD camera for imaging GFP fusion proteins in yeast cells is sensitivity. The CCD camera, with high-efficiency detectors, proper cooling, and slow-scan readout, can accumulate light from the wide field microscope over long exposure periods without building up significant noise to degrade the image. Taking 3-s exposures with 2 × 2 binning at 1–10% of maximum excitation generates 50–250 gray levels above the noise floor of 20–30 gray levels. The major noise components, after background subtraction, are autofluorescence from the cell and media and the photon counting noise. A signal-to-noise ratio of between 1.5 : 1 and 5 : 1 produces an acceptable image of microtubules. Growth was not impaired by this level of shuttered 490-nm excitation and imaging was limited by eventual photobleaching. Shorter (1-s) exposures, using maximum fluorescence excitation, killed the cells within 15 min but indicated that there is little movement of the dynein–GFP–labeled microtubules during the 3-s exposure. Hence, we use low levels of irradiance, which are not harmful to the cell, and gain sensitivity by "on-chip integration" of the signal for 3 s.

Confocal microscopy has been successfully used to image larger cells having higher total concentrations of GFP fusion protein. Confocal imaging requires very strong illumination, usually a laser, because the majority of the fluorescence emission is discarded and because the efficiency of the photomultiplier tubes used as detectors is low (often 10%). The high level of excitation is phototoxic to yeast and photobleaches the GFP rapidly. Confocal microscopy, however, is useful for immunofluorescence studies in yeast because of the tremendous signal amplification derived from having many fluorochrome-containing antibodies bound to a single copy of the protein of interest.

VI. Image Acquisition and Processing

Given that the haploid yeast approximates a sphere of about 5–8 μm in diameter, and the depth of field of one fluorescence image from a wide-field microscope is about 1 μm, we developed a routine to image the entire cell. Using a computer controlled Z-motor, five images of 3-s exposure are taken for each time point (usually 1-min intervals). Briefly, the stage is moved up 2 μm and then moves down in 1-μm steps to −2 μm, taking a fluorescence image at each step. A single DIC image is taken when the state is at the zero position. The stage then returns to the zero (starting) position. The background (average of 25 3-s exposures taken with the camera shutter closed) is subsequently subtracted

from the fluorescence images. A maximum projection is then made from each set of five fluorescence images. The DIC and fluorescence images can now be montaged or overlaid for display. It should be noted that measurements are done by using the nonprojected images to preserve accuracy in three dimensions (Shaw *et al.*, 1997a).

VII. Applications and Examples: Expression of Dynein–GFP *in Vivo*

The dynein–GFP fusion protein allowed us to visualize the dynamic behavior of the microtubule cytoskeleton and the spindle poles. TEM descriptions of cellular physiology and anatomy (Byers, 1981; Byers and Goetsch, 1975) were unable to clearly define the ultrastructure of budding yeast astral microtubules. Antitubulin immunostaining and DAPI on fixed cells greatly enhanced observation, but fixation methods still left astral microtubules incomplete (Adams and Pringle, 1984; Pringle *et al.*, 1989). Expression of a GFP-tagged dynein within the yeast cell (Shaw *et al.*, 1997b), as well as GFP-tagged tubulin (Carminati and Stearns, 1997), produced the first view of the dynamic and physiological role for astral microtubules *in vivo*. Though the single images of astral microtubules and the nucleus look very similar to fixed cell photographs, putting the images into motion provides critical new information, especially with regard to dynamic processes such as mitosis.

Early forays into kinetic studies of *in vivo* processes in *Saccharomyces cerevisiae* used only DIC (Jones *et al.*, 1993; Koning *et al.*, 1993; Yang *et al.*, 1997; Yeh *et al.*, 1995). The addition of multimode time-lapse imaging of GFP fusion proteins (Kahana *et al.*, 1995; Salmon *et al.*, 1998; Shaw *et al.*, 1997a) enabled kinetic analysis at the molecular level. The addition of multimode, time-lapse images of spindle elongation reveals that the transition from a sausage-shaped to a bilobed-shape nucleus, observed in DIC (Yeh *et al.*, 1995), is accompanied by the separation of the chromatin, observed using the DNA intercalating dye, DAPI (see Fig. 4 in Shaw *et al.*, 1997a). We also see that in the heart-shaped stage, observed in DIC (lower cell at 15 min, Shaw *et al.*, 1997a, Fig. 4), the spindle pole fits into the cleft of the heart shape. Additionally, astral microtubules emanating from the spindle poles at either end of the nucleus exhibit dynamic instability throughout anaphase. Astral microtubules >2 μm in length are occasionally observed but do not maintain this length for more that the 1-min interval of the original time-lapse series (Shaw *et al.*, 1997b).

Altering protein complex stoichiometry can reveal information about protein function not apparent from traditional genetic analysis. Extreme overexpression of the dynein–GFP (8 hr of induction) had unexpected consequences for the integrity of the spindle pole. In 2 of the 14 cells we imaged that had dynein–GFP levels 15- to 20-fold higher than normal, we observed a fragmentation of the

spindle pole body (Fig. 3). MTOC fragmentation did not occur in cells expressing other GFP fusion proteins, regardless of expression level [tubulin–GFP, cyclin–GFP, and nuf2–GFP (S. Shaw and K. Bloom, unpublished results)]. Time-lapse imaging revealed that the astral microtubules attached to the new fragment were dynamic and that the fragment center remained in proximity to the nucleus, represented by the dark area in the cell in Fig. 3. Spindle elongation occurs between the two original spindle poles oriented along the mother bud axis, with no apparent regard for the new fragment.

A role for dynein in spindle pole organization has been demonstrated for animal cells by reconstitution of spindle components in an *in vitro* extract system (Walters and Salmon, 1997) and *in vivo* by injection of components of the dynein

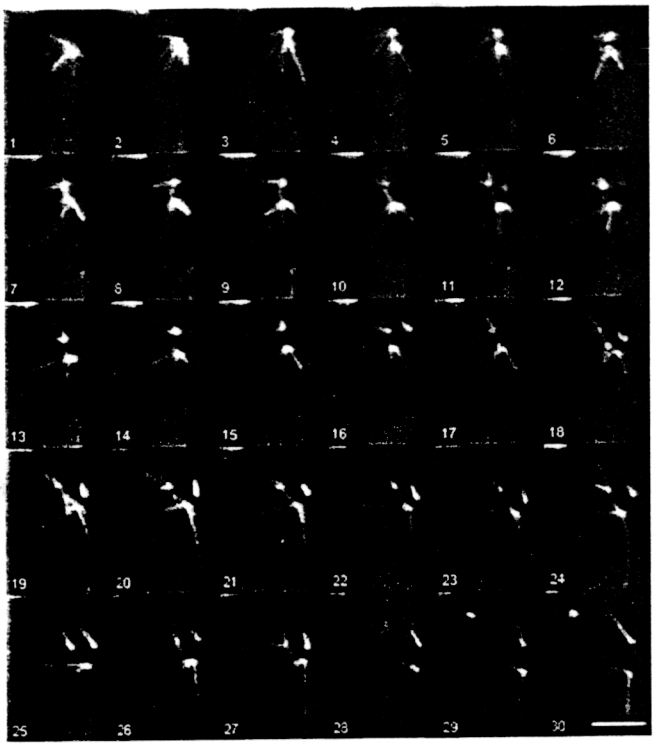

Fig. 3 Fragmentation of the spindle pole body in a cell overexpressing dynein–GFP. A time-lapsed series (3-min intervals shown) of a large budded cells, with bud facing down and out of the micrograph, containing extremely high dynein–GFP levels. Astral microtubules are hyperelongated but remain dynamic. Separation of spindle poles (1–6) is followed by the fragmentation of the pole distal to the bud with the fragment appearing to the right (11–16). Note that the astral microtubules emanating from the new spindle pole remain dynamic. Astral microtubules from the bud-proximal pole remain oriented into the bud (19–30) as the nucleus undergoes anaphase in the mother cell (28–30). Spindle elongation appears to involve only the two original spindle poles and not the new fragment. Scale bar = 5 μm.

Fig. 4 Dynein–GFP overexpression during mating in *S. cerevisiae*. Zygote and first bud mating are shown. The bud extends toward the upper left corner. Arrows mark three spindle bodies where only two are expected. Scale bar = 5 μm.

or dynactin complexes (p50: Echeverri *et al.*, 1996). A complex of proteins, including dynein and dynactin, has been postulated to organize the pole. Multiple proteins tether a large number of microtubules to the relatively small centrosomes (Waters and Salmon, 1997). No function for dynein at the spindle pole has been found in yeast even though dynein decorates each pole (Eshel *et al.*, 1993; Li *et al.*, 1993; Shaw *et al.*, 1997b) (Fig. 4). The occasional fragmentation of the MTOC in the presence of a vast excess of dynein–GFP may suggest a role for dynein in maintaining MTOC cohesion in yeast as well as mammalian cells.

Early attempts to image the kinetics of cell cycle progression with DIC microscopy led to the establishment of critical kinetic parameters of the cell division process and to mitosis in particular. The advent of multimode imaging together with the utility of the GFP allow *in vivo* analysis and kinetic parameters to be explored for the entirety of proteins comprising the yeast genome.

References

Adams, A. E. M., and Pringle, J. R. (1984). Relationship of actin and tubulin distribution to bud growth in wild-type and morphogenetic-mutant *Saccharomyces cerevisiae*. *J. Cell Biol.* **98**, 934–945.

Amberg, D. C., Zahner, J. E., Mulholland, J. W., Pringle, J. R., and Botstein, D. (1997). Aip3p/Bud6p, yeast actin-interacting protein that is involved in morphogenesis and the selection of bipolar budding sites. *Mol. Biol. Cell* **8,** 729–753.

Bi, E., Maddox, P., Lew, D. J., Salmon, E. D., McMillan, J. H., Yeh, E., and Pringle, J. R. (1998). Roles of a nonessential actomyosin contractile ring and of the septins in *Saccharomyces cerevisiae* cytokinesis. Submitted for publication.

Byers, B. (1981). *In* "The Molecular Biology of the Yeast *Saccharomyces:* Life Cycle and Inheritance" (J. N. Strathern, E. W. Jones, and J. R. Broch, eds.), pp. 59–96. Cold Spring Harbor Laboratory Press, Cold Spring Harbor, NY.

Byers, B., and Goetsch, L. (1975). Behavior of spindles and spindle plaques in the cell cycle and conjugation of *Saccharomyces cerevisiae. J. Bacteriol.* **124,** 511–523.

Carminati, J. L., and Stearns, T. (1997). Microtubules orient the mitotic spindle in yeast through dynein-dependent interactions with the cell cortex. *J. Cell Biol.* **138,** 629-641.

Cottingham, F. R., and Hoyt, M. A. (1997). Mitotic spindle positioning in *Saccharomyces cerevisiae* is accomplished by antagonistically acting microtubule motor proteins. *J. Cell Biol.* **138,** 1041–1053.

Dezwaan, T. M., Ellingson, E., Pellman, D., and Roof, D. M. (1997). Kinesin-related KIP3 of *Sacchromyces cerevisiae* is required for a distinct step in nuclear migration. *J. Cell Biol.* **138,** 1023–1040.

Echeverri, C. J., Paschal, B. M., Vaughan, K. T., and Vallee, R. B. (1996). Molecular characterization of the 50-kD subunit of dynactin reveals function for the complex in chromosome alignment and spindle organization during mitosis. *J. Cell Biol.* **132,** 617–633.

Eshel, D., Urrestarazu, L. A., Vissers, S., Jauniaux, J. C., van Vliet-Reedijk, J. C., Planta, R. J., and Gibbons, I. R. (1993). Cytoplasmic dynein is required for normal nuclear segregation in yeast. *Proc. Natl. Acad. Sci. USA* **90,** 11172–11176.

Etcheverry, T. (1990). *Methods Enzymol.* **185,** 319–329.

Finger, F. P., Hughes, T. E., and Novick, P. (1998). Sec3p is a spactial landmark for polarized secretion in budding yeast. *Cell* **92,** 559–571.

Futcher, B., and Carbon, J. (1986). Toxic effects of excess cloned centromeres. *Mol. Cell. Biol.* **6,** 2213–2222.

Hinnebusch, A. G. (1992). *In* "The Molecular and Celluar Biology of the Yeast *Saccharomyces*" (E. W. Jones, J. R. Pringle, and J. R. Broach, eds.), pp. 319–414. Cold Spring Harbor Laboratory Press, Cold Spring Harbor, NY.

Inoué, S., and Spring, K. (1997). *Video Microscopy,* 2nd ed. Plenum, New York.

Jones, E. W., and Fink, G. R. (1982). *In* "The Molecular Biology of the Yeast *Saccharomyces:* Metabolism and Gene Expression" (J. N. Strathern, E. W. Jones, and J. R. Broach, eds.), pp. 181–299. Cold Spring Harbor Laboratory Press, Cold Spring Harbor, NY.

Jones, H. D., Schliwa, M., and Drubin, D. G. (1993). Video microscopy of organelle inheritance and motility in budding yeast. *Cell Motil.* **25,** 129–142.

Kahana, J. A., Schnapp, B. J., and Silver, P. A. (1995). Kinetics of spindle pole body separation in budding yeast. *Proc. Natl. Acad. Sci. USA* **92,** 9707–9711.

Koning, A. J., Lum, P. Y., William, J. M., and Wright, R. (1993). DiOC6 staining reveals organelle structure and dynamics in living cells. *Cell Motil. Cytoskel.* **25,** 111–128.

Li, Y. Y., Yeh, E., Hays, T., and Bloom, K. (1993). Disruption of mitotic spindle orientation in a yeast dynein mutant. *Proc. Natl. Acad. Sci. USA* **90,** 10096–10100.

Lippincott, J., and Li, R. (1998). Sequential assembly of myosin II, an IQGAP-like protein, and filamentous actin to a ring structure involved in budding yeast cytokinesis. *J. Cell Biol.* **140,** 355–366.

Longtine, M. S., McKenzie, A., III, Demarini, D. J., Shah, N. G., Wach, A., Brachat, A., Philippsen, P., and Pringle, J. R. (1998). Additional modules for versatile and economical PCR-based gene deletion and modification in *Saccharomyces cerevisiae. Yeast* **14,** 953–961.

Moreland, R. B., Langevin, L. L., Singer, R. H., Garcea, R. L., and Hereford, L. M. (1987). Amino acid sequences that determine the nuclear localization of yeast histone 2B. *Mol. Cell. Biol.* **7,** 4048–4057.

Mumberg, D., Muller, R., and Funk, M. (1994). Regulatable promoters of *Saccharomyces cerevisiae:* Comparison of transcriptional activity and their use for heterologous expression. *Nucleic. Acids Res.* **22,** 5767–5768.

Niedenthal, R. K., Riles, L., and Hegeman, J. H. (1996). Green fluorescent protein as a marker for gene expression and subcelluar localization in budding yeast. *Yeast* **12,** 773–786.

Patterson, G., and Piston, D. (1998). Quantitative imaging of TATA-binding protein (TBP) in living yeast cells. Submitted for publication.

Pringle, J. R., Preston, R. A., Adams, A. E. M., Stearns, T., Drubin, D. G., Haarer, B. K., and Jones, E. W. (1989). Fluorescence microscopy methods for yeast. *Methods Cell Biol.* **31,** 338–437.

Resnick, M. A., Westmoreland, J., and Bloom, K. (1990). Heterogeneity and maintenance of centromere plasmid copy number in *Saccharomyces cerevisiae*. *Chromosoma* **99,** 281–288.

Salmon, E. D., Inoué, T., Desai, A., and Murray, A. W. (1994). High resolution multimode digital imaging system for mitosis studies in vivo and in vitro. *Biol. Bull.* **187,** 231–232.

Salmon, E. D., Shaw, S. L., Waters, J., Waterman-Storer, C. M., Maddox, P. S., Yeh, E., and Bloom, K. (1998). *In* "Methods in Cell Biology: Video Microscopy" (G. Sluder and D. D. Wolf, eds.), Vol. 56. Academic Press, London.

Shaw, S. L., Yeh, E., Bloom, K., and Salmon, E. D. (1997a). Imaging green fluorescent protein fusion proteins in *Saccharomyces cerevisiae*. *Curr. Biol.* **7,** 701–704.

Shaw, S. L., Yeh, E., Maddox, P., Salmon, E. D., and Bloom, K. (1997b). Astral microtubule dynamics in yeast: A microtubule-based searching mechanism for spindle orientation and nuclear migration into the bud. *J. Cell Biol. 139,* 985-994.

Solomon, F., (1991). *Annu. Rev. Cell Biol.* **7,** 633–662.

Straight, A. F., Belmont, A. S., Robinett, C. C., and Murray, A. W. (1996). GFP tagging of budding yeast chromosomes reveals that protein–protein interactions can mediate sister chromatid cohesion. *Curr. Biol.* **6,** 1599–1608.

Straight, A. F., Marshall, W. F., and Murray, A. W. (1997). Mitosis in living budding yeast: Anaphase a but no metaphase plate. *Science* **277,** 574.

Waters, J. C., and Salmon, E. D. (1997). Pathways of spindle assembly. *Curr. Opin. Cell Biol.* **9,** 37–43.

Yang, S. S., Yeh, E., Salmon, E. D., and Bloom, K. S. (1997). Identification of a mid-anaphase checkpoint in budding yeast. *J. Cell Biol.* **136,** 345–354.

Yeh, E., Skibbens, R. V., Cheng, J. W. Salmon, E. D., and Bloom, K. (1995). Spindle dynamics and cell cycle regulation of dynein in the budding yeast, *Saccharomyces cerevisiae*. *J. Cell Biol.* **103,** 687–700.